Child's Nervous System (2019) 35:833–841
https://doi.org/10.1007/s00381-019-04119-x

ORIGINAL ARTICLE

Upward movement of cerebrospinal fluid in obstructive hydrocephalus—revision of an old concept

Hans C. Bock[1] · Steffi F. Dreha-Kulaczewski[2] · Awad Alaid[1] · Jutta Gärtner[2] · Hans C. Ludwig[1]

Received: 25 February 2019 / Accepted: 8 March 2019 / Published online: 27 March 2019

Abstract

Purpose The specific pathophysiological processes in many forms of obstructive hydrocephalus (HC) are still unclear. Current concepts of cerebrospinal fluid (CSF) dynamics presume a constant downward flow from the lateral ventricles towards subarachnoid spaces, which are in contrast to neurosurgical observations and findings of MRI flow studies. The aim of our study was to analyze CSF movements in patients with obstructive HC by neuroendoscopic video recordings, X-ray studies, and MRI.

Methods One hundred seventeen pediatric patients with obstructive HC who underwent neuroendoscopy in our center were included. Video recordings were analyzed in 85 patients. Contrast-enhanced X-rays were conducted during surgery prior to intervention in 75 patients, and flow void signals on pre-operative MRI could be evaluated in 110 patients.

Results In 83.5% of the video recordings, CSF moved upwards synchronous to inspiration superimposed by cardiac pulsation. Application of contrast medium revealed a flow delay in 52% of the X-ray studies prior to neurosurgery, indicating hindered CSF circulation. The appearances and shapes of flow void signals in 88.2% of the pre-operative MRI studies suggested valve-like mechanisms and entrapment of CSF.

Conclusions Neuroendoscopic observations in patients with obstructive HC revealed upward CSF movements and the corresponding MRI signs of trapped CSF in brain cavities. These observations are in contrast to the current pathophysiological concept of obstructive HC. However, recent real-time flow MRI studies demonstrated upward movement of CSF, hence support our clinical findings. The knowledge of cranial-directed CSF flow expands our understanding of pathophysiological mechanisms in HC and is the key to effective treatment.

Keywords Hydrocephalus · Neuroendoscopy · Real-time flow MR imaging · CSF dynamics

Introduction

Hydrocephalus (HC) is defined as a disturbance of cerebrospinal fluid (CSF) formation, flow, or absorption, leading to accumulation of fluid and increase of CSF spaces in the central nervous system (CNS). Underlying etiologies of these processes are still vastly unknown. Early pathophysiologic concepts of HC were derived from works of Dandy, Key, and Retzius [6, 7]. Based on their studies, the choroid plexus (CP) was established as the site of CSF production and arachnoid villi in the large venous sinuses as the structures of its absorption. They concluded that CSF movements occur from the lateral ventricle downward trough the 3rd and 4th ventricles and their delicate interconnections. Blockage of this continuous downward fluid flow had been determined to cause the dilation of CSF spaces cranial to the obstruction. In

Steffi F. Dreha-Kulaczewski and Hans C. Bock contributed equally to this work.

Electronic supplementary material The online version of this article (https://doi.org/10.1007/s00381-019-04119-x) contains supplementary material, which is available to authorized users.

✉ Hans C. Ludwig
hludwig@med.uni-goettingen.de

[1] Department of Neurosurgery, Section Pediatric Neurosurgery, University Medical Center Göttingen, Robert-Koch-Str. 40, 37075 Göttingen, Germany

[2] Department of Pediatrics and Adolescent Medicine, Division of Pediatric Neurology, University Medical Center Göttingen, Robert-Koch-Str. 40, 37075 Göttingen, Germany

contrast to these obstructive or non-communicating HC forms, they established the category of communicating HC induced by diminished CSF absorption.

Over the last decades, major advances in the knowledge of CSF function and dynamics have significantly broaden our view on its physiology. Perivascular spaces, cranial, and spinal nerve sheaths have been established as the main CSF outflow routes by, e.g., Murtha et al. [5, 13, 22, 26]. Moreover, advances in MRI techniques over the last decades have facilitated new insights into CSF flow and expanded our understanding of its physiologic and disturbed circulation [21, 40]. In clinical routine, the appearance of flow void signals on conventional T2-weighted MR images within dilated CSF spaces serves as the essential criteria to differentiate between mechanical obstruction and malabsorption as cause for the HC [1, 30]. The majority of MR studies of CSF dynamics so far used cine phase-contrast (pc) flow MRI with cardiac gating [1, 19]. Mainly, they focused on the oscillating CSF flux in the aqueduct craniocaudally during systole and in reverse direction during diastole.

More recently, novel real-time pc flow MRI techniques at high spatial and temporal resolution allow measurements independent of cardiac synchronization. Applying this MR technique, forced inspiration has been identified as the main driving force of CSF flow in healthy subjects [10]. More importantly, an upward movement of CSF towards the brain was observed in response to every forced inhalation. Thereby, the CSF system counterbalances the enhanced venous outflow out of the cranial cavity to ensure a constant intracranial volume in accordance with the Monro-Kellie doctrines [8] [11] [12]. CSF moving cranial from the 3rd ventricle towards the lateral ventricles through the aqueduct has been demonstrated not only by real-time flow MRI but also by microsurgical and neuroendoscopic procedures and intracranial monitoring [25]. These observations of a cranial flow direction are in strong contrast to the prevailing notion of a continuous downward fluid flux.

The aim of our study was to analyze CSF movements in patients with obstructive HC. Comprehensive retrospective analyses of our patient data acquired from neurosurgical procedures, X-ray, and MR imaging were performed to determine CSF flow dynamics.

Patients and methods

Patients

Between 1997 and 2015, neuroendoscopic surgeries were performed in 117 patients (age range 0.1–18 years, mean 5.5 ± 5.4 SD; 43 female) in the Pediatric Neurosurgery at our Medical Center. All patients were diagnosed with obstructive HC arising from hindrances of the CSF pathway at varying locations and of different types. As listed in detail in the Supplementary table, the HC was categorized as obstructive HC ($n = 54$) or loculated HC ($n = 46$), among which three had an isolated 4th ventricle. Fourteen patients showed tumor-related HC, and three HCs were caused by arachnoid cysts. More specifically, obstruction was provoked by aqueductal stenosis (45/54 patients) or a stenosis of Monroi foramen (13/54 patients). Loculated HC was caused by prematurity-related hemorrhage (mean gestational age: 28 weeks) in 33/46 patients. Arachnoid cysts were located temporal in the three patients and fenestrated by endoscopically assisted microsurgery. The tumors blocking the CSF circulation at the aqueduct originated from the tectal plate or were classified as ocular pathway gliomas as well as craniopharyngeomas.

Ventriculo-peritoneal (VP) shunt systems had been in place in 27/117 patients prior to the neuroendoscopy reported here. Implantation of a VP shunt during the neuroendoscopy was necessary in 42/117 patients. In 18/33 patients with loculated HC due to post-hemorrhagic HC (PHHC), a stent catheter was implanted connecting iatrogenic membrane fenestrations of different CSF compartments and the CSF pathway draining into the shunt device.

Under standard analgo-sedation, patients were ventilated routinely using intermittent positive airway pressure ventilation (IPPV) with age-specific parameters, i.e., positive end-expiratory pressure (PEEP) ≤ 5 mmHg under routine monitoring. None of the patients had cardiac or pulmonary diseases.

All patients, procedures, and MR-imaging data were collected prospectively and analyzed retrospectively as well as prospectively using the institutional hydrocephalus registry [2], and informed consent was obtained from patients or their caregivers. The institutional review board of the Georg-August-University Goettingen approved the study. It was in compliance with the Declaration of Helsinki.

Methods

Neurosurgical procedures

The neurosurgical techniques used are summarized in the Supplementary table. Endoscopic third ventriculostomies (ETV) were performed in 45 patients and fenestration of cysts (CF) in 42. Another 13 patients benefitted from a septal pellucidotomy (SP) to restore CSF circulation. Isolated 4th ventricles were reconnected to the ventricular system by aqueductoplasties and a stent catheter. The temporal arachnoid cysts were treated by endoscopically assisted microscopy. In 14 patients with tumor-related obstructive HC, various neuroendoscopic procedures were used to restore CSF circulation.

Fenestrations of separating membranes during SP, CF, and ETV were conducted using a fiber-guided near-infrared

Thulium-laser (Revolix®, Lisa laser products, Katlenburg, Germany) [24, 33] inserted into rigid endoscopes (Storz LittleLotta® and Pediscope® Aesculap). All cases were assisted by neuronavigation (Brainlab®, Heimstetten, Germany).

Informed written consent was obtained from all parents or guardians for the surgical procedures.

Intraoperative recordings of CSF dynamics

Video recordings

In 85/117 procedures, intraoperative video documentation (Storz Aida® System, Tuttlingen, Germany) could be obtained. Membrane movements, fluctuations, and cranial-directed flow of tissue fragments after opening the membranous structures were considered indicators for previous CSF entrapment. Ventilation cycle and heart action during surgery were registered by observation of the thoracic movements as well as of the respirator and pulse curves during monitoring.

Contrast enhanced C-arc X-rays

In 75/117 patients, 2–5 ml of contrast medium (Solutrast®) were applied into the irrigation channel of the endoscope for a lateral C-arc X-ray view to evaluate the extent of aqueductal obstruction and to test whether a patent communication towards the basal cisterns or across the obstructive membrane was created. CSF enhancement following application of the contrast medium was monitored qualitatively (Fig. 1a, b). Of note, single images were taken by X-ray radioscopy to observe the contrast enhancement of CSF space connections.

MR-imaging

All patients underwent a pre-operative structural MRI study. Follow-up examinations were conducted 3 months after surgery in accordance with clinical guidelines.

Pre-operative MRI studies were carried out in the Institute of Neuroradiology at our University Medical Center Göttingen in 110/117 patients. Until 2005, 24/110 patients were investigated at a 1.5-T MRI scanner and 86 patients later at a 3-T scanner. For 7/117 patients, referring hospitals conducted the MRI. All follow-up MRI examinations were performed at our institution.

Signs of CSF flow were assessed on T2-weighted images of pre- and corresponding post-operative MRI-studies (see Supplementary table for details). MR features indicative of an entrapment of CSF prior to surgery were categorized as specified in Table 1.

Results

Intraoperative findings of CSF dynamics

Video recordings

The side of occlusion of the CSF pathway could directly be visualized via video recording in 55/85 procedures (Supplementary table). In 30/85 procedures, neuroendoscopic surgery was aimed at other structures than the sites of occlusion. After opening the obstructive membranous structure, periodic fluctuations of residual membranes and tissue particles parallel to inspiration during IPP ventilation could be found in 71/85 patients (Table 2). In 14/85 recordings, no

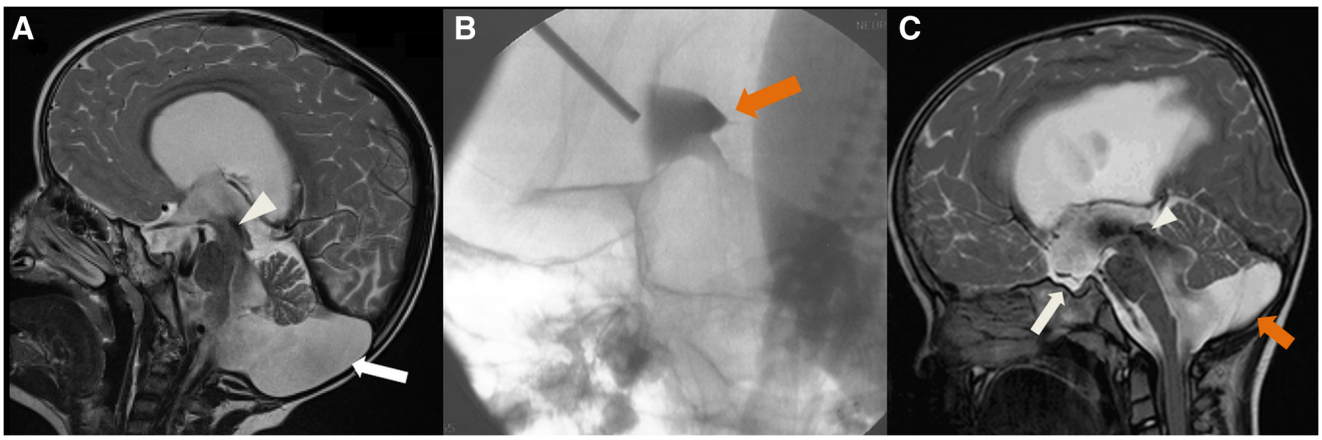

Fig. 1 Hydrocephalus caused by enlarged infratentorial CSF containing spaces. **a** Large Dandy Walker cyst (white arrow) on sagittal T2-weighted image with enlarged ventricular system and flow void (white arrow head) within the small aqueduct. **b** Intraoperative lateral C arc X-ray of the same patient as in **a** after application of contrast medium. Contrast medium appears trapped within the 3rd ventricle (orange arrow) and has not yet exchanged with CSF spaces. Note the endoscope extending into the 3rd ventricle. **c** Sagittal T2-weighted image demonstrating hydrocephalus with expansion of all ventricles, bulged floor of the 3rd ventricle (white arrow), strong flow void in the widened aqueduct (arrow head), and an enlarged CSF containing space in the posterior fossa (MRI category 2, see Table 1) (orange arrow) before endoscopic thirdventriculostomy

Table 1 MRI categories for features of CSF entrapment in obstructive hydrocephalus

Category	MRI features
1	Large supratentorial ventricles
	Small aqueduct with weak flow void
	Small 4th ventricle
	Bulged floor of the 3rd ventricle indicating aqueductal stenosis
2	Large supratentorial ventricles
	Bulged floor of 3rd ventricle
	Obstruction by infratentorial CSF containing space
3	Sparse/missing flow void in the aqueduct on pre-ETV MRI
	Pronounced flow void on 3 months post-ETV MRI
4	Blockade of Monroi foramen
	Unilateral HC
	Flow void at the hindrance with shape suggestive of upward flow
5	Enlarged 4th ventricle
	Flow void at the floor of the 4th ventricle
	Incomplete aqueductal stenosis
6	Loculated CSF cysts
	Differences in size between ventricular and cystic cavities

ETV: endoscopic thirdventriculostomy

entrapment or obstruction of CSF flow movements was identifiable.

In all of the 45 patients of the ETV subgroup, tissue flotations and motions of small particles at the edges of the stoma's fenestrations upwards and towards the endoscope were seen. After aqueductoplasty for correcting aqueduct stenosis in three patients, upwardly directed motions of membrane rims (see Supplementary Video) were visible. The dynamics clearly was synchronous to ventilation and superimposed heart action with the maximum deflection during concurrent systolic pulse and end-inspiratory phase.

Contrast-enhanced C-arc X-rays

During 75 neurosurgical procedures, contrast medium was applied into one of the lateral ventricles to enhance visualization of CSF movements. Prior to the surgical intervention, 39/75 procedures yielded restricted and delayed CSF flow to the 4th ventricle and parapontine cisterns (see Fig. 1b, Table 2, and Supplementary table). Flow lag observed prior to the intervention was considered as an indicator of hindered circulation, thus entrapped CSF. After opening the floor of the 3rd ventricle or obstructive membranes, contrast medium turbulences following ventilation-related flux could be distinguished in 39/75 procedures. The contrast agent in the remaining 36/75 patients revealed no signs of flow obstruction though affirmed free communication of CSF compartments on lateral C-arc X-ray projections.

MR-Imaging

The qualitative evaluation of MRIs of 110/117 patients obtained prior to surgery as well as the 117 MRIs acquired 3 months after surgery is summarized in Table 2 and Supplementary table. Seven pre-operative MRIs could not be classified, because they were lost or incomplete due to missing T2-weighted sagittal imaging.

Figures 1 to 6 demonstrate representative T2-weighted images of each of the six categories. MRI features of category 1 with aqueductal stenosis as displayed in Fig. 2a were found in 32/110 pre-operative MRIs. Large ventricles due to infratentorial obstruction could be observed in 6/110 MRIs prior to surgery and were classified as category 2 (Fig. 1a, c). Category 3 required a pronounced alteration from the pre-operative to the post-ETV flow conditions. The appearance of a strong flow void through the new stoma and the aqueduct was seen in 8/45 ETVs (Fig. 2c). The five patients with unilateral HC caused by blockade of one Monroi foramen revealed a flow void suggestive of upward CSF motion (Fig. 3). They were classified in category 4. Flow voids at the bottom of an enlarged 4th ventricle and stenosis of the aqueduct (Fig. 4a), defined as category 5, could be identified in two patients. Partially isolated 4th ventricle with multiple cystic compartments and complete isolation of the 4th ventricle with obstruction in the infratentorial CSF space are illustrated by Fig. 4b, c, respectively. Category 6 comprised most of the patients (53) revealing distended loculated CSF cysts as depicted in Fig. 5. Interestingly, in

Table 2 Assessment of CSF dynamics in three modalities: intraoperative video recording, contrast enhanced C-arc X-ray, and MRI

Modality	No. of patients	Results	No. of patients	%
Intraoperative video	85	CSF flow upward +	71	83.5
		CSF flow upward −	14	
Contrast enhancedC-arc X-ray	75	CM flow lag* +	39	52
		CM flow lag* −	36	
Pre-operative MRI	110	Trapping signs +	97	88.2
		Trapping signs −	13	

No. of patients: number of patients with study results available for analysis; %: percentage of patients with signs of upward movement of CSF and CSF entrapment; *CM*: contrast medium; +: signs present; −: signs not detectable; *: prior to surgical intervention

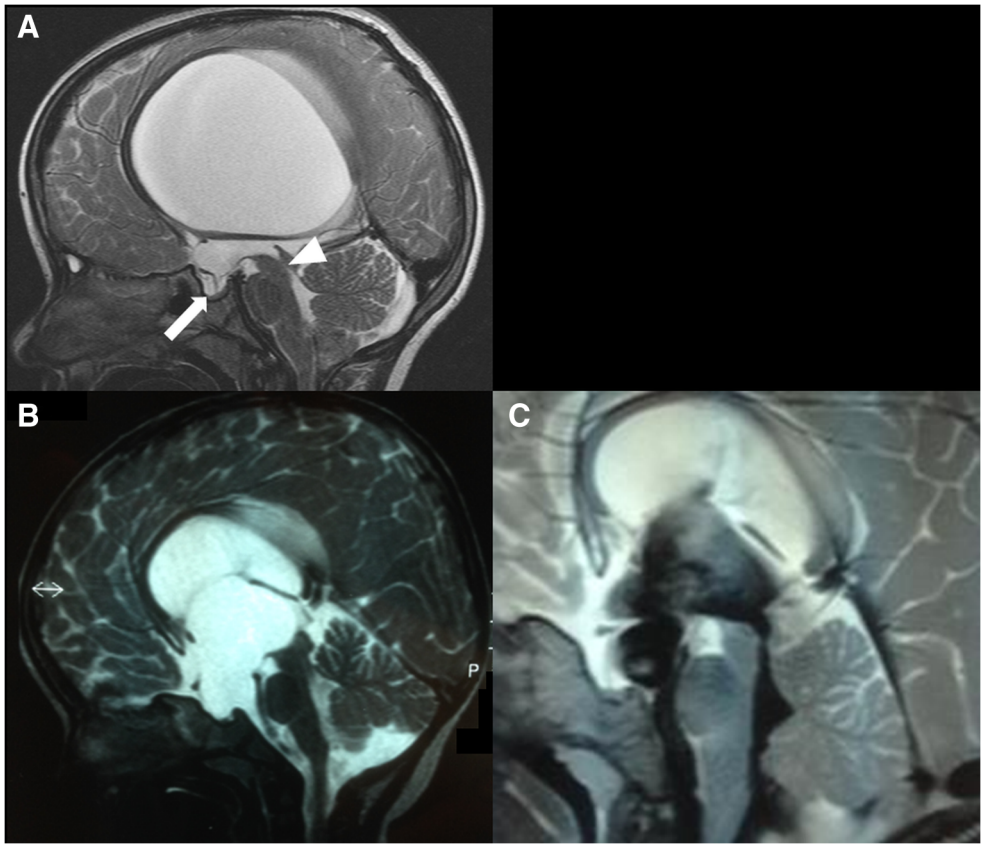

Fig. 2 Hydrocephalus due to aqueductal stenosis. **a** Sagittal T2-weighted image with characteristic signs of an aqueductal stenosis, i.e., enlarged lateral and 3rd ventricles and bulged floor of the 3rd ventricle (arrow); very sparse flow void in the aqueduct (arrow head); altogether indicative of CSF trapping within the ventricles due to the severely yet not completely occluded aqueduct (MRI category 1, s. Table 1). **b** Sagittal T2-weighted image with similar signs of an aqueductal stenosis as in **a** in another patient. **c** Same patient as in **b** 3 months after endoscopic thirdventriculostomy. Note the strong flow void signal in praepontine cistern, stoma, aqueduct, and 4th ventricle (MRI category 3, s. Table 1)

patients with midbrain tumors blocking the aqueduct completely, no enlargement of the ventricles cranial to the tumor localization could be detected (Fig. 6).

Overall, the qualitative analysis of the flow void signals in standard T2-weighted MRI revealed upward CSF movements and trapping mechanisms prior to surgery in 88.2% of all analyzed patients (see Table 2).

In summary, results from all three technical modalities could be obtained in 59/117 patients (Supplementary table). The 106/117 patients showed CSF entrapment in at least one of these methods. In two of the remaining 11 patients, none of the modalities indicated fluid entrapment. Results available from only one or two modality in five patients failed to show fluid trapping, and in four patients, no data from the three modalities could be included.

Discussion

Up to today, obstructive HC is considered to arise from a blockage of CSF flow downstream of its production site and consecutive dilatation of the CSF spaces above. Novel findings of real-time flow MRI studies however demonstrated significant, inspiratory induced upward flow of CSF in healthy subjects, which is in contrast to these current, controversial pathophysiological concepts. Here, we investigated CSF dynamics in a thoroughly defined cohort of 117 pediatric patients with obstructive HC to reevaluate the underlying pathophysiology. Standard neurosurgical procedures, namely intraoperative video recordings and contrast-enhanced C-arc X-rays during neuroendoscopic surgery, were applied in combination with corresponding pre- and post-operative T2-weighted MRIs.

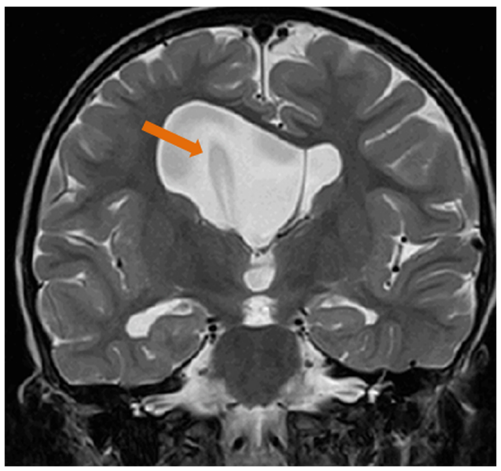

Fig. 3 Occlusion of one Monroi foramen leads to unilateral hydrocephalus. Sagittal T2-weighted image shows enlarged right lateral ventricle caused by a blockade of the right Monroi foramen. Shape of the flow void in the lateral ventricle suggests upward flow direction (MRI category 4, s. Table 1) (orange arrow)

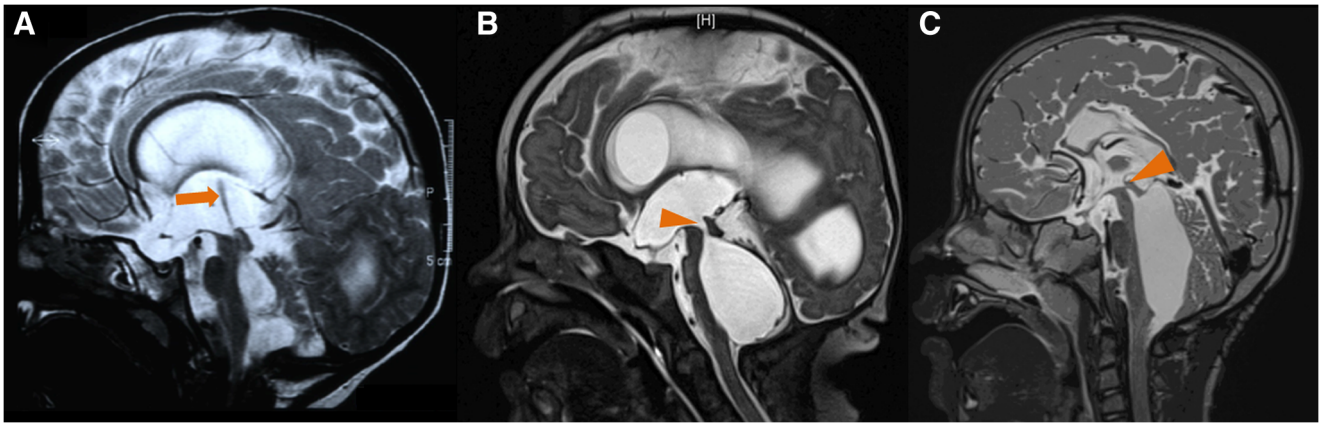

Fig. 4 Isolated 4th ventricles. Sagittal T2-weighted images of two preterm children with post-hemorrhagic hydrocephalus and partially isolated 4th ventricle (**a**, **b**). **a** Shape of the strong flow void (orange arrow) within aqueduct and 3rd ventricle is suggestive of upward flow direction and high velocity. **b** Sparse flow void (orange arrowhead) indicating flow although at lower scale (MRI category 5, s. Table 1). **c** Sagittal T2-weighted image of another preterm child displaying a completely isolated, enlarged, elongated, and distended 4th ventricle and aqueductal stenosis (orange arrow head). Third and lateral ventricles are of normal size

Distinct signs of a cranially directed CSF flow were found in 83.5% of the video recordings obtained during neuroendoscopy. In fact, intraoperative tissue fluctuations followed cardiac pulsation; however, respiration at frequencies defined by IPP ventilation provoked the dominant effects. Thus, the movements of CSF seemed to adhere to the characteristic intracranial pressure curves [25]. Flow lag of contrast agent, indicative of hindered CSF flux, was identified in 52% of the X-ray studies prior to surgery. The distribution of contrast medium followed more a pattern of mixing and diffusion rather than a directed much less caudally directed CSF flow in 36/75 patients. The low temporal resolution of the C-arc X-ray methodology might explain this considerable number. Furthermore, only very few X-ray images are usually required to visualize an altered flow pattern of the contrast agent after surgery and to verify the patency of the established CSF pathways.

In line with the neurosurgical observations, 88.2% of the corresponding pre-operative MRI studies revealed features consistent with CSF entrapment in enlarged brain cavities. Moreover, appearances and the shapes of flow voids were suggestive of cranial fluid flow. Results of the intervention were

Fig. 5 Loculated CSF cysts adjacent to the ventricular system. Multiple loculated cystic compartments on axial T2-weighted image. CSF filled cysts of various size are abutted bilaterally to the body and posterior horns of the lateral ventricles. The large cyst in the right hemisphere appears distended and "inflated" (MRI category 6, s. Table 1). Note the striking difference in size compared with the slit-like anterior horns (arrows)

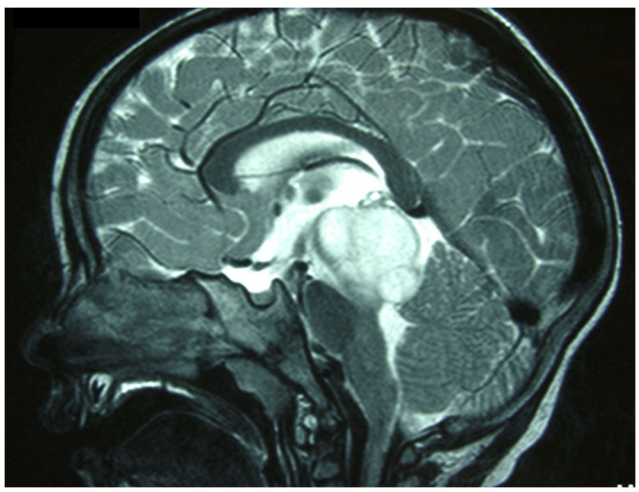

Fig. 6 Midbrain tumor causing complete blockage of the aqueduct. Midbrain tumor in this sagittal T2-weighted image causes complete blockage of the aqueduct. Of note, the ventricles are of normal size not enlarged. The complete blockage may prevent CSF entrapment or valve mechanisms

depicted on post-operative T2-weighted MRIs demonstrating new flow void signals along the CSF pathways or ETV.

Based on the intraoperative and MRI results, it can be postulated that trapping of the CSF results from strong upward motion driven by forced inspiration and valve-like hindrances along the pathways. Taken together, the clinical findings support recent real-time flow MRI studies, demonstrating cranial CSF flux from the spinal canal into the cranial vault, through the aqueduct up into 3rd ventricle synchronous to forced inspiration [11, 12].

Pulsatile CSF movements following cardiac action and respiration have also previously been observed, e.g., by Greitz et al. and Williams et al. [18, 34, 37–39]. Early myelography studies showed an ascent of the jodipine column during inspiration and a descent during expiration first published 1941 [31]. More recently, Ringstad [32] reported observations obtained by gadobutrol instillation into the lumbar arachnoid CSF space in patients with normal pressure hydrocephalus (NPH), which he could demonstrate entering the 4th ventricle as early as 60 min after application and further promotion into all ventricles after 24 h in supine position [32]. This must be interpreted as a directed movement from the spinal CSF spaces into the cranial ventricles.

Animal experiments inserting a systolic synchronized pumping balloon into the ventricular system of lambs (8–10 kg of weight) resulted in development of ventriculomegaly without any ICP elevation [29] [9]. This could be explained by the immaturity of CSF pathways [28] in very young 3-week-old lambs used for the study. Furthermore, CSF resorption rates into the extracranial lymphatic system of sheep can reach values as high as 50% of the fluid [3]. Ventricular dilation caused by a pumping balloon mechanism but without raising the ICP could be explained by the assumption of an ependymal CSF flow and a pressure sensing mechanism. This has been attributed to the sensing cilia of the ependyma, which is able to differentiate circadian circumstances [14], flow directions, and flow velocities. Disturbances of the sensing cilia system are responsible for alterations in ventricular morphology and dimension [15].

Another important theory about CSF dynamics established by Greitz et al. [20] [19] focused on hemodynamic influences based on Dandy's pioneering work. Expansion of the intracranial arteries during systole was assumed to lead to an expulsion of venous blood out of the brain tissue and into the large venous sinuses. Consequently, piston-like motions of the CP within the main cisterna and at the foramen magnum prompted the pulsatile motions of cervical CSF. The oscillations of CSF synchronous to the heart beat as shown by cardiac-gated flow MRI supported this theory. Meanwhile, this observation has been recently excluded as a main CSF moving force [35].

Flow-sensitive MRI studies later avoiding cardiac-gating demonstrated the effects of respiration on CSF dynamics [16, 23, 40]. In the study by Chen et al., significant CSF flux during inspiration was detected in the subarachnoid spaces in addition to cardiac-related components [4]. Inspiration results in reduction of intrathoracic pressure and thus enhances the outflow of venous blood out of the head towards the heart. The upward surge of CSF counterbalances this increased venous outflow to avoid hemodynamic or pressure changes to the brain in accordance with the Monro-Kellie doctrine [11].

The CSF moving upward into the ventricles must pass exclusively through the aqueduct. Implying the small aqueduct to be a tubular system with laminar flow, the flow volume therefore should obey the law of Hagen-Poiseuille according to which the inside radius of a tube enters the equation in the fourth power. Thus, it could be hypothesized that the aqueduct acts as a tightly regulated valve system adapting CSF flow rates into the supratentorial brain ventricles by only small adjustments to its diameter. Recent studies using pc-MRI could demonstrate that the cardiac-driven CSF velocity in the aqueduct was higher than the one prompted by respiration. On the other hand, a larger CSF volume was displaced by the respiratory compared with the cardiac component [36]. Both effects are responsible for the characteristic ICP-curve, which reflects fast systolic and diastolic curves superimposed by slower respiratory effects during spontaneous as well as ventilated breathing [25]. When the peak of the CSF velocity (cardiac component) and the volume displacement (respiratory component) coincide, the valve mechanism of an obstruction might open hence leading to trapping of the CSF.

Stenosis possessing valve-like mechanisms alongside CSF pathways may exclusively permit upward flux and hence trap fluid inside brain ventricular cavities and cysts, leading to obstructive HC.

It is of note that the intraoperative video recordings and X-rays were obtained under ventilation, which constitutes seemingly different conditions, then real-time flow MRI was performed. However, standard PEEP in cardio-pulmonary healthy subjects has no clinically significant effect on central venous and intracranial pressures [17]. Furthermore, pleural pressures remained negative during the inspiratory cycles of IPPV as Novak et al. demonstrated in dogs [27]. Thus, also under standard IPPV, both venous and CSF flow are driven by respiratory pressure changes within the thoracic cavity.

Conclusion

Our findings in patients with obstructive HC revealed CSF upward movements and MRI signs of trapped fluid in brain cavities, which are in line with results from real-time flow MRI. Unraveling the direction of CSF flow in health and in pathological conditions like obstructive HC has enormous therapeutic impact. It is of eminent importance in HC with structural malformation and stenosis along the CSF pathways,

which may act like one-way valves to define effective neurosurgical interventions, e.g., ETV, fenestration of membranes, aqueductoplasties, or stent maneuvers. Moreover, future real-time flow MRI studies will include not only patients with obstructive HC but also those with other conditions due to perturbed CSF circulation like spontaneous intracranial hypotension and syringomyelie to unravel pathomechanisms and to open new options for therapies and respective evaluations.

Conflict of interest The authors declare that they have no competing interest.

Author contributions HCB and AA performed the endoscopic part of the studies. HCL designed the study, conducted the study including endoscopies, and wrote the manuscript. SDK conducted the study and wrote the manuscript. JG conducted the study and wrote the manuscript.

References

1. Bhadelia RA, Madan N, Zhao Y, Wagshul ME, Heilman C, Butler JP, Patz S (2013) Physiology-based MR imaging assessment of CSF flow at the foramen magnum with a valsalva maneuver. Am J Neuroradiol 34(9):1857–1862
2. Bock HC, Kanzler M, Thomale U-W, Ludwig H-C (2018) Implementing a digital real-time hydrocephalus and shunt registry to evaluate contemporary pattern of care and surgical outcome in pediatric hydrocephalus. Childs Nerv Syst 34(3):457–464
3. Boulton M, Flessner M, Armstrong D, Hay J, Johnston M (1998) Determination of volumetric cerebrospinal fluid absorption into extracranial lymphatics in sheep. Am J Phys 274(1 Pt 2):R88–R96
4. Chen L, Beckett A, Verma A, Feinberg DA (2015) Dynamics of respiratory and cardiac CSF motion revealed with real-time simultaneous multi-slice EPI velocity phase contrast imaging. Neuroimage 122(C):281–287
5. Chen L, Elias G, Yostos MP, Stimec B, Fasel J, Murphy K (2014) Pathways of cerebrospinal fluid outflow: a deeper understanding of resorption. Neuroradiology 57(2):139–147
6. Dandy WE (1919) Experimental hydrocephalus. Ann Surg 70:129–142
7. Dandy WE (1938) The operative treatment of communicating hydrocephalus. Ann Surg 108:194–202
8. Delaidelli A, Moiraghi A (2017) Respiration: a new mechanism for CSF circulation? J Neurosci 37(30):7076–7078
9. Di Rocco C, Pettorossi VE, Caldarelli M, Mancinelli R, Velardi F (1978) Communicating hydrocephalus induced by mechanically increased amplitude of the intraventricular cerebrospinal fluid pressure: experimental studies. Exp Neurol 59:40–52
10. Dreha-Kulaczewski S, Joseph AA, Merboldt K-D, Ludwig H-C, Gärtner J, Frahm J (2015) Inspiration is the major regulator of human CSF flow. J Neurosci 35(6):2485–2491
11. Dreha-Kulaczewski S, Joseph AA, Merboldt K-D, Ludwig H-C, Gärtner J, Frahm J (2017) Identification of the upward movement of human cerebrospinal fluid in vivo and its relation to the brain venous system. J Neurosci 37(9):2754–16–2402
12. Dreha-Kulaczewski S, Konopka M, Joseph AA, Kollmeier J, Merboldt K-D, Ludwig H-C, Gärtner J, Frahm J (2018) Respiration and the watershed of spinal CSF flow in humans. Sci Rep 8(1):5594–5597
13. Edsbagge M, Tisell M, Jacobsson L, Wikkelsö C (2004) Spinal CSF absorption in healthy individuals. Am J Physiol Regul Integr Comp Physiol 287(6):R1450–R1455
14. Faubel R, Westendorf C, Bodenschatz E, Eichele G (2016) Cilia-based flow network in the brain ventricles. Science 353(6295):1–4
15. Foerster P, Daclin M, Asm S, Faucourt M, Boletta A, Genovesio A, Spassky N (2017) mTORC1 signaling and primary cilia are required for brain ventricle morphogenesis. Development 144(2): 201–210
16. Friese S, Hamhaber U, Erb M, Klose U (2004) B-waves in cerebral and spinal cerebrospinal fluid pulsation measurement by magnetic resonance imaging. J Comput Assist Tomogr 28(2):255–262
17. Funk DJ, Jacobsohn E, Kumar A (2013) The role of venous return in critical illness and shock-part I: physiology. Crit Care Med 41(1): 255–262
18. Greitz D (1993) Cerebrospinal fluid circulation and associated intracranial dynamics. A radiologic investigation using MR imaging and radionuclide cisternography. Acta Radiol Suppl 386:1–23
19. Greitz D, Wirestam R, Franck A, Nordell B, Thomsen C, Ståhlberg F (1992) Pulsatile brain movement and associated hydrodynamics studied by magnetic resonance phase imaging. The Monro-Kellie doctrine revisited. Neuroradiology 34(5):370–380
20. Greitz D (2004) The hydrodynamic hypothesis versus the bulk flow hypothesis. Neurosurg Rev 27(4):1–2
21. Kelly EJ, Yamada S (2016) Cerebrospinal fluid flow studies and recent advancements. Semin Ultrasound CT MRI 37:92–99
22. Klarica M, Oresković D, Bozić B, Vukić M, Butković V, Bulat M (2009) New experimental model of acute aqueductal blockage in cats: effects on cerebrospinal fluid pressure and the size of brain ventricles. NSC 158(4):1397–1405
23. Klose U, Strik C, Kiefer C, Grodd W (2000) Detection of a relation between respiration and CSF pulsation with an echoplanar technique. J Magn Reson Imaging 11(4):438–444
24. Ludwig HC, Kruschat T, Knobloch T, Teichmann H-O, Rostasy K, Rohde V (2007) First experiences with a 2.0-microm near infrared laser system for neuroendoscopy. Neurosurg Rev 30(3):195–201–discussion 201
25. Ludwig HC, M K, Timmermann A, Weyland W (2000) The influence of airway pressure changes on intracranial pressure (ICP) and the blood flow velocity in the middle cerebral artery (VMCA). Anasthesiol Intensivmed Notfallmed Schmerzthe 35:141–145
26. Murtha LA, Yang Q, Parsons MW, Levi CR, Beard DJ, Spratt NJ, McLeod DD (2014) Cerebrospinal fluid is drained primarily via the spinal canal and olfactory route in young and aged spontaneously hypertensive rats. Fluids Barriers CNS 11(1):12
27. Novak R, Matuschak GM, Pinsky M (1988) Effect of positive-pressure ventilatory frequency on regional pleural pressure. J Appl Physiol 65:1314–1323
28. Oi S, Di Rocco C (2006) Proposal of "evolution theory in cerebrospinal fluid dynamics" and minor pathway hydrocephalus in developing immature brain. Childs Nerv Syst 22(7):662–669
29. Pettorossi VE, Di Rocco C, Mancinelli R, Caldarelli M, Velardi F (1978) Communicating hydrocephalus induced by mechanically increased amplitude of the intraventricular cerebrospinal fluid pulse pressure: rationale and method. Exp Neurol 59:30–39
30. Qvarlander S, Ambarki K, Wåhlin A, Jacobsson J, Birgander R, Malm J, Eklund A (2016) Cerebrospinal fluid and blood flow patterns in idiopathic normal pressure hydrocephalus. Acta Neurol Scand 135(5):576–584
31. Reitan H (2013) On movements of fluid inside the cerebro-spinal space. Acta Radiol Orig Ser 22(5–6):762–779
32. Ringstad G, Vatnehol SAS, Eide PK (2017) Glymphatic MRI in idiopathic normal pressure hydrocephalus. Brain 140(10):2691–2705
33. Schuhmann MU, Kural C, Lalla L, Ebner FH, Bock C, Ludwig H-C (2019) 2-micron continuous wave laser assisted neuroendoscopy: clinical experience of two institutions in 524 procedures. World Neurosurg 122:e81–e88

34. Spijkerman JM, Geurts LJ, Siero JCW, Hendrikse J, Luijten PR, Zwanenburg JJM (2018) Phase contrast MRI measurements of net cerebrospinal fluid flow through the cerebral aqueduct are confounded by respiration. J Magn Reson Imaging 40:2583–2512
35. Takizawa K, Matsumae M, Hayashi N, Hirayama A, SANO F, Yatsushiro S, Kuroda K (2018) The choroid plexus of the lateral ventricle as the origin of CSF pulsation is questionable. Neurol Med Chir (Tokyo) 58(1):23–31
36. Takizawa K, Matsumae M, Sunohara S, Yatsushiro S, Kuroda K (2017) Characterization of cardiac- and respiratory-driven cerebrospinal fluid motion based on asynchronous phase-contrast magnetic resonance imaging in volunteers. Fluids Barriers CNS 14(1):25
37. Williams B (1981) Simultaneous cerebral and spinal fluid pressure recordings. Acta Neurochir 59(1–2):123–142
38. Williams B (1981) Simultaneous cerebral and spinal fluid pressure recordings. Acta Neurochir 58(3–4):167–185
39. Williams H (2008) A unifying hypothesis for hydrocephalus, Chiari malformation, syringomyelia, anencephaly and spina bifida. Cerebrospinal Fluid Res 5:7
40. Yamada S, Miyazaki M, Yamashita Y, Ouyang C, Yui M, Nakahashi M, Shimizu S, Aoki I, Morohoshi Y, McComb J (2013) Influence of respiration on cerebrospinal fluid movement using magnetic resonance spin labeling. Fluids Barriers CNS 10(1): 36